Environmental Nanotechnology, Monitoring & Management 5 (2016) 62–73

Contents lists available at ScienceDirect

Environmental Nanotechnology, Monitoring & Management

journal homepage: www.elsevier.com/locate/enmm

Macrogel and nanogel networks based on crosslinked poly (vinyl alcohol) for adsorption of methylene blue from aqua system

Kamel Rizq Shoueir[a,*], Ali Ali Sarhan[a], Ayman Mohamdy Atta[b], Mageda Ali Akl[a]

[a] Chemistry Department, Faculty of Science, Mansoura University, Mansoura, Egypt
[b] Surfactant Research Chair, Chemistry Department, College of Science, King Saud University, Saudi Arabia

ARTICLE INFO

Article history:
Received 19 December 2015
Received in revised form 19 March 2016
Accepted 30 March 2016

Keywords:
Macrogel
MB adsorption
PVA nanogel
Thermodynamic

ABSTRACT

Two different types of network were synthesized. Semi-IPN macrogel type PVA@P(AMPS-*co*-AAc) (SIMT) and PVA- EPC@P(AMPS-*co*-AAc) (100 nm) nanogel (CCPNT). Poly (vinyl alcohol) (PVA) was used as matrix and copolymerized 2-acrylamido-2-methyl-1-propane- sulfonic acid (AMPS), Acrylic acid (AAc) based materials were used in the removal of methylene blue (MB). Epichlororhydrine (EPC) was used as crosslinker to link the CCPNT. The maximum removal for MB was observed at (10AAc-*co*-90AMPS) (wt.:wt. %) monomer ratio for both networks. The prepared macro and nanogel materials were characterized by SEM, BET, TEM and DLS. The adsorption followed pseudo-second-order kinetics and fit Langmuir-type isotherm. The adsorption capacity was found to be equal to 416.6 mg/g, 181.8 mg/g for CCPNT and SIMT, respectively.

1. Introduction

Dyes and pigments are widely used as coloring agents. The total dye consumption in the textile industry worldwide is more than 10.000 ton/year. It is estimated that 2% of the produced dyes annually discharged in effluent due to manufacturing processes while 10% is discharged from textile and associated industries (Betul et al., 2013; Allen and Koumanova, 2005). The release of colored waste water from these industries may present an eco-toxic hazard and potential danger of bioaccumulation was obtained, which can eventually affect man through the food chain (Shengfang et al., 2011). Methylene blue (MB) is a thiazine cationic dye, can cause eye burns. On inhalation it can cause short periods of difficult and rapid breathing while ingestion through mouth may cause nausea, vomiting, and methemoglobinemia (Hameed et al., 2007). Therefore, the treatment is an interest due to its harmful impacts on receiving waters.

Adsorption has been differential as a potential technology for the removal of dyes from wastewater compared with other conventional methods suitable for the treatment of textile industry effluent, adsorption is preferred technique due to simplicity and flexible design and easy operation. Moreover, the adsorption process may generate little or no toxic pollutants during treatment and operating costs (Crini, 2006; Auta and Hameed, 2012). Moreover, it doesn't have environment issues as it does not produce any sludge (Vecino et al., 2015a).

Polymer gels are a special class of macromolecular networks that contain a large segment of solvent within their structure. They are mainly useful for biomedical applications because of their ability to mimic biological tissues such as alginate and cellulosic residues (Vecino et al., 2015b). In response to external environmental stimuli like pH and temperature, the gels can reversibly swell or shrink up to 1000 times in volume, and have varied applications such biomimetic, biosensors, artificial muscles, chemical separation, biomaterials, cell culture systems, catalysis, photonics, drug delivery systems and separation purpose (Murray and Snowden, 1995; Chilkoti et al., 2002; Biffis, 2001; Morris et al., 2016; Kiser et al., 2000; Peppas et al., 2000; Reese et al., 2004; Wu et al., 2011). Because of their surface area, perfect mechanical strength, adjustable surface chemistry, feasibility regeneration under mild conditions and efficient pore size distribution (Qu, 2008; Gupta and Suhas, 2009; Ngaha et al., 2011; Pan et al., 2009). Gels can be made either in bulk or in micro or nanoparticles.

Hydrogel nanoparticles adsorbent has gained much attention due to the readily removal ability with the formation of Nano-network upon absorption of pollutants from aqueous solution due to presence of ionic groups in the backbone that opens potential area of different applications related to remove pollutants from

* Corresponding author at: Polymer Laboratory, Chemistry Department, Faculty of Science, Mansoura University, ET- 35516,Mansoura, Egypt.
E-mail addresses: kameltag@yahoo.com (K.R. Shoueir), Ali_Ali_sarhan@yahoo.com (A.A. Sarhan), khaled_atta00@yahoo.com (A.M. Atta), Magedaakl@yahoo.com (M.A. Akl).

http://dx.doi.org/10.1016/j.enmm.2016.03.001

wastewaters (Perez-Ameneiro et al., 2015; Jiuhui, 2008), where hydrogels complex with metal ions through the functional groups (i.e., —COOH, —C=O(NH_2), —SH, —COO—, —NH_2, and —OH) in their network. In particular, PVA is a water- soluble linear polymer, which is employed in practical applications in the field of separation processes (Abdeen et al., 2015; Magda et al., 2013; Dragan and Apopei, 2011). It was reported that, the strong acidic monomer 2-acrylamido-2-methyl propane-1-sulfonic acid, (AMPS) comprises a strongly ionizable sulfonate group which acquire its hydrogel high chelating ability (Akl et al., 2016; Rivas et al., 2003). AMPS were used in the synthesis of many hydrogels to form hydrogelized with hydrophilic acrylic monomers such as acrylic acid (Souda and Sreejith, 2015) and acrylamide (Ömer et al., 2006). The incorporation of PVA in certain macrogel type or nanogel type ensure its excellent mechanical strength, and the chemical crosslinking is required to create and modify polymer nanostructure, where the properties can be improved, such as thermal, mechanical and chemical stabilities (Mandal et al., 2012). Moreover, PVA content in the gels type gives higher affinity to crosslink formation through the intra- and/or intermolecular hydrogen bonding via —H groups. Therefore, the purpose of this study was to prepare two types of network dimensions, where PVA as a template and either the first semi-IPN hydrogels composed of AMPS-*co*-AAc in macro type and the second IPN-AMPS-AAc in Nano scale. There used to evaluate the dye sorption properties for methylene blue (MB) from aqueous solution.

2. Experimental

2.1. Materials

Monomers, i.e., Acrylic acid (AAc, purified by rectify, purchased from Across), 2-acrylamido-2-methyl-1-propane-sulfonic acid (AMPS, purchased from Across), *N*-methylenebisacrylamide (MBA, from Fluka), redox initiator i.e., ammonium persulfate (APS, from Fluka), polymer. i.e., Poly (vinyl alcohol) (PVA, polymerization degree is 1750 +50, purchased from Across), Epichlorohydrin (EPC; Fluka). Methylene blue (MB, were obtained from Merck) and used without further purification. Other reagents were grade and used as received.

2.2. Synthesis of semi IPN-macrogel type (SIMT)

10 ml of prepared gelatinized PVA (70 °C, for 40 min) was added to the following mixture; AAc weighing 0.72 g (90 wt.%), then 0.23 g (10 wt.%) AMPS added and dissolved in 5 ml water. After these additions, 1% concentration of MBA (0.0095 g/1 ml) and aqueous solutions of 0.5 wt. % of redox initiator APS (0.0048 g/1 ml) with respect to mount of monomers and crosslinker, 1% concentration of TEMED were added to these aqueous solutions. Similarly take 0.08 g AAc (10 wt.%) and 2.07 g AMPS (90 wt.%) to identify the higher functionality uptake, 0.021 g MBA (1%/1 ml), 0.01 g APS (0.5 wt.%) and 1% TEMED. The whole reaction for the two sets lasted for 1 h under N_2 gas, the solution was transferred into petri-dish, in order to prepare gels in the shape of the film, the gels were cut into pieces prior to use.

2.3. Synthesis of chemically crosslinked PVA nanoparticles type (CCPNT)

1 wt.% of PVA was dissolved in 100 ml of distilled water. A solution of 0.66 g NaOH in 5 ml of water was slowly added till pH 12 via syringe with vigorous stirring. Then added 15 ml of acetone drop wise with stirring for 30 min, the solution was cooled at 10 °C for 24 h and it became weak blue, indicating that the long chains of PVA shrank to nanoparticles. The precursor solution with 50 ml of PVA nanogel was mixed with 1 ml EPC and 50 ml of the same synthesized ratio (10AAc-*co*%) and (90AAc-*co*-10AMPS) (wt.:wt.%) macrogel solution and heated with stirring at 100 °C for 3 h under N_2 atmosphere to produce nanogel structure. The obtained dispersed nanogels was separated by precipitation into 10 folds of acetone and redispersed in water forming nanoparticle dispersion

2.4. Measurements

(10AAc-*co*-90AMPS) (wt.:wt.%) nanogel was selected for characterization. TEM micrograph analysis of colloidal nanogel particle was taken using a JEOL JEM-2100 electron microscope. The sample prepared by adding acetone to the aqueous solution till the solution became slightly turbid.

The surface area and pore radius determinations were based on isotherms of adsorption-desorption isotherms of N_2 gas at 77 K using Micrometrics gas adsorption analyzer (Nova 3200 USA) of macro and nanogel were estimated using the BET method. The pore radius was determined using BJH method. The sample was degassed under vacuum at 200 °C for 4 h, using 0.1 g sample prior to surface area measurements.

The size distribution of CCPNT was determined using photon correlation spectroscopy technique (PCS) (Malvern Instruments Ltd.).

The concentration of the MB was measured using a UV/spectrophotometer (Schimadzu UV-1208 model).

2.5. MB decolonization tests

The ability of the hydrogel types to adsorb MB from an aqueous solution was determined at room temperature and under a constant stirring rate 300 rpm. Adsorption studies have been carried out using a batch equilibrium technique. Thus, weighed amount 0.01 g of dried hydrogel types were placed in a two flasks and contacted with 10 ml of aqueous solution of the MB with concentrations ranging from 10 to 1000 mg/l. The initial solution pH was studied by adjusting MB solutions (C_o, 100 mg/l) to varied pH_o values (2.0, 4.0, 6.0, 8.0 and 10.0) with 0.1 mol/l HCl or NaOH solution using a pH meter (Sartorius, PB-10). For kinetic study, 100 mg/l of MB solutions (10 ml, pH_o 6) were agitated with 0.01 g of hydrogels at 25 °C at time intervals 5 to 200 min. The dye solution was isolated from the adsorbent by centrifugation at 300 rpm for 15 min. The absorbency of samples was measured using the mentioned spectrophotometer at a wavelength corresponding to the maximum absorbance, about 665 nm for cationic MB. Then the concentrations of the samples were determined by finally using a calibration curve for MB over a range of concentrations. The amount of dye adsorbed onto macro and Nano-gels, q_e (mg/g), was calculated by the following mass balance equation:

$$q_e = \frac{\left(C_i - C_f\right).V}{m} \quad (1)$$

where q_e (mg/g) represents the amount of MB adsorbed onto the gels; C_i and C_f are MB initial and the concentration at equilibrium; respectively (mg/l), V(ml) the volume of the solution (l), and m (g) is the weight of the adsorbent used.

3. Results and discussion

3.1. Preparation of SIMT

During polymerization in aqua system primary radicals are generated by initiation of the redox initiator (APS) and monomers i.e. AAc, AMPS and MBA. Radicals are also generated on PVA and it takes part in propagation reactions of the monomers (Mandal et al., 2012; Dhara et al., 1999). Thus, SIMT is formed from growing radicals of

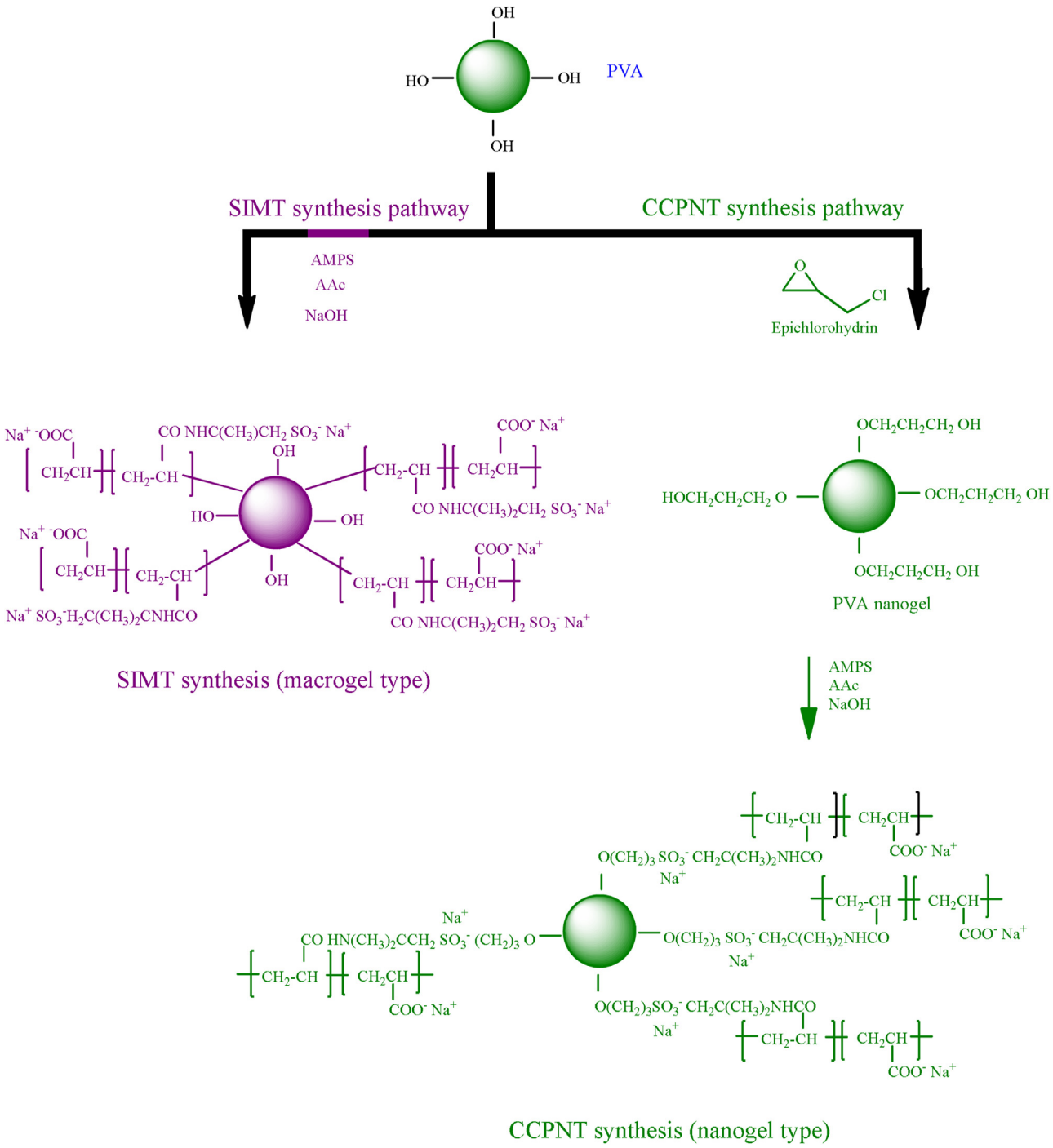

Scheme 1. Synthesis of SIMT (left hand side) and CCPNT (right hand side).

monomers and PVA macroradicals. Possible structure of the SIMT is shown in left hand side of Scheme 1.

3.2. Preparation of CCPNT

Although acetone and water are miscible, the cosolvent becomes poor solvent for PVA chains (Yao et al., 2009), moreover introducing EPC as a chemically crosslinked onto PVA chains leading to aggregated globules to form PVA/EPC nanogels. Carboxylic acid groups in PAAc and sulfonic acid groups in PAMPS easily hydrolyze under alkaline conditions generating COO^- and $SO3^-$ respectively (Jie et al., 2013). The possible mechanism of the polymerization is presented in the right hand side of Scheme 1.

3.3. Characterization of SIMT and CCPNT

Fig. 1(a) shows the cross-sectional structure, highly pores and gaps network structure in character to form well-known interconnected, three-dimensional porous network was observed, and this is due to the expanded network can be generated by electrostatic repulsions among PVA hydroxyl groups during the polymerization process and COO^-, $SO3^-$ groups. Thus, the response rate could be greatly enhanced by the incorporation PVA into the SIMT network.

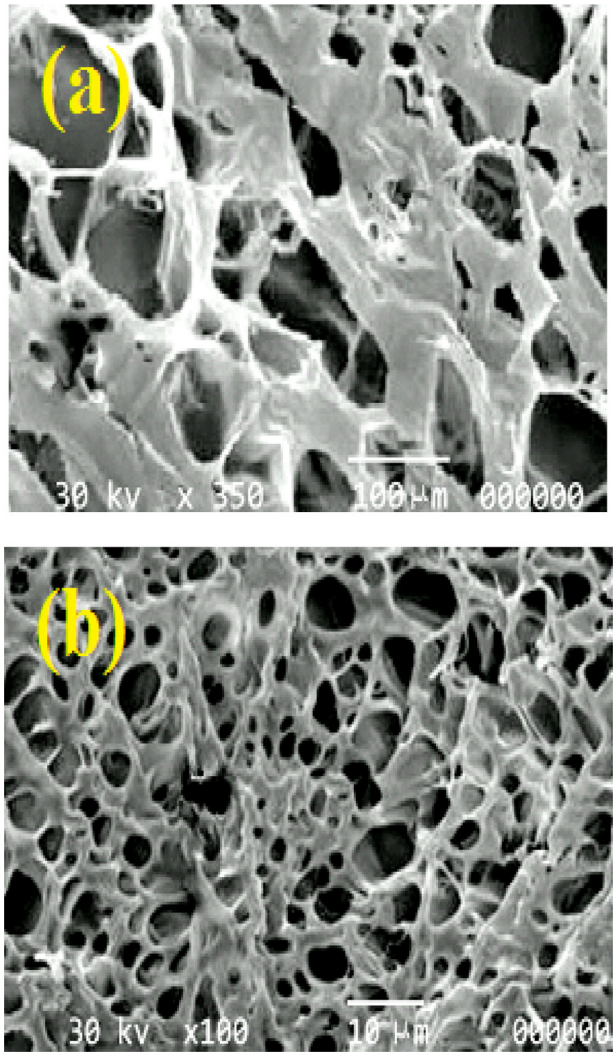

Fig. 1. SEM images of cross-section, (a) SIMT, (b) CCPNT.

Fig. 1(b) the SEM image of nanogel shows a clear influence of the chemical crosslinking of PVA on the gel morphology. Thus, the nanogel formed via EPC more porous structure and smaller particles act as a connection between larger ones, help to attach and fix them in the matrix. As the polymerization reaction proceeds above 70 °C maximum micro pore were formed on the surface of the CCPNT. Formation of dense layer could be avoided and thus we could able to increase the affinity towards diffusivity and removal behaviors (Magdy et al., 2012). As a consequence, the pores which survived look lower than those of the hydrogel type.

Fig. 2(a,b) shows the TEM of crosslinked PVA nanogel in mixed (water/acetone). There are some changes from its initial coil or agglomerate caddice-like unattached particulates, and a rope-like configuration with aggregates of about 50 nm in diameter, which indicated that PVA nanoparticles could be formed in a mixed solvent of water/acetone (Yao et al., 2009). Fig. 2(c) shows the addition of P(AAc-*co*-AMPS) to PVA nanogels. The structure of the nanoparticles was greatly influenced by the addition of (AAc-*co*-AMPS) comonomer concentration in solution; large number of nanospheres was observed by TEM. Therefore, the formation of the PVA/PAMPS complex nanogel is due to the polymerization of AAc and AMPS monomers with the collapsed PVA as a template or core at their LCST to produce well-defined core shell nanogels (Wu et al., 2011). The nanogel was 100 nm in diameters. This behavior is due to two effects, the first one is the high compatibility of

Table 1
Surface characteristics comparison between SIMT and CCPNT.

Characteristic		SIMT	CCPNT
1	Total pore volume summary		
	Total pore volume (cc/g)	0.75	3.39
2	BJH desorption summary		
	Surface Area (m^2/g)	**613.8**	**1047.4**
	Pore volume (cc/g)	0.80	5.25
	Pore radius Dv(r)	8.29 A°	11.60 A°
3	Average Pore Size summary		
	Average pore radius	3.4 nm	5.3 nm

comonomer with the PVA matrix, leading to the agglomeration of the nanogel, so that the interface area between commoner and PVA is maximized. The second effect is the resultant surfactant-free PVA-PAA-PAMPS nanogel exhibit the temperature volume phase transition behaviors (VPTT) in water from the swollen state converted to the collapsed state as the temperature increases. This effect can be also used for colloidal stable core/shell particles with small nanoparticles (Risheng et al., 2011).

Fig. 3 shows the particle size analysis of nanogel. The particle size was around 100 nm with a hardship distribution which illustrated from particle size histograms. The smaller particles have higher surface area/volume ratio, which makes it pave for the adsorption of MB. The smaller particles will have a greater adsorption affinity for MB. In contrast, larger particles, which allow the slow adsorption behavior. The expected size distribution, which is entered prior to the analysis, is fitted with a predetermined particle size distribution from the measured by TEM

Examining the data related to the surface parameters of SIMT/CCPNT and according to the IUPAC classification of the hysteresis (IUPAC, 1985), in our case it can be assimilated with H2 type for macro/nanogel as clearly in Fig. 4. In a simplified manner, this hysteresis is generally attributed to a difference in mechanism between condensation/evaporation processes creating in pores with narrow necks and wide bodies, but it is assured that network effects have an important role (Wu et al., 2011). The relative pressure range is 0.4–0.9, implying the presence of meso-pores in both gel samples (Peng et al., 2011).

Table 1, shows the surface characteristics of gel types. There are appreciable differences were observed between the surface areas of two gel types. It was observed that porosity rely on the volume of the pores present in the SIMT/CCPNT scaffolds. In nanogel formulation maximum porosity was found having required chemically cross-linking density strong enough to keep the optimized volume of pores while in hydrogel due to the incorporation of the higher crosslink density within the polymer structure leads to decrease in pore volume. The average pore radius determined from the desorption isotherm were 3.4 and 5.3 nm for SIMT and CCPNT, respectively. This might be justified by the complexity of factors that may have opposite effects on surface properties of the nanogel (chemical crosslinking degree, the presence of polar groups and hydrogen bonding degree, pore shape, sorption type, etc.).

3.4. Adsorption of MB onto SIMT and CCPNT

3.4.1. Effects of monomer ratio on removal of MB

The effect of increasing AAc/AMPS mol ratio on the adsorption capacity of MB was studied by varying the AAc/AMPS ratio as shown in Fig. 5. Increasing the AMPS concentration at monomer feed composition from 10 wt.% to 90 wt.%, increased the adsorption capacity up to 94.23% rather than 81.56% removal for 90 wt.% AAc. With these results, it is possible to understand that the increase of AMPS concentration in the media would result in the increment of homo copolymerization and crosslinking, consequently adsorption increase. Moreover, AMPS have polar groups like —CONH and

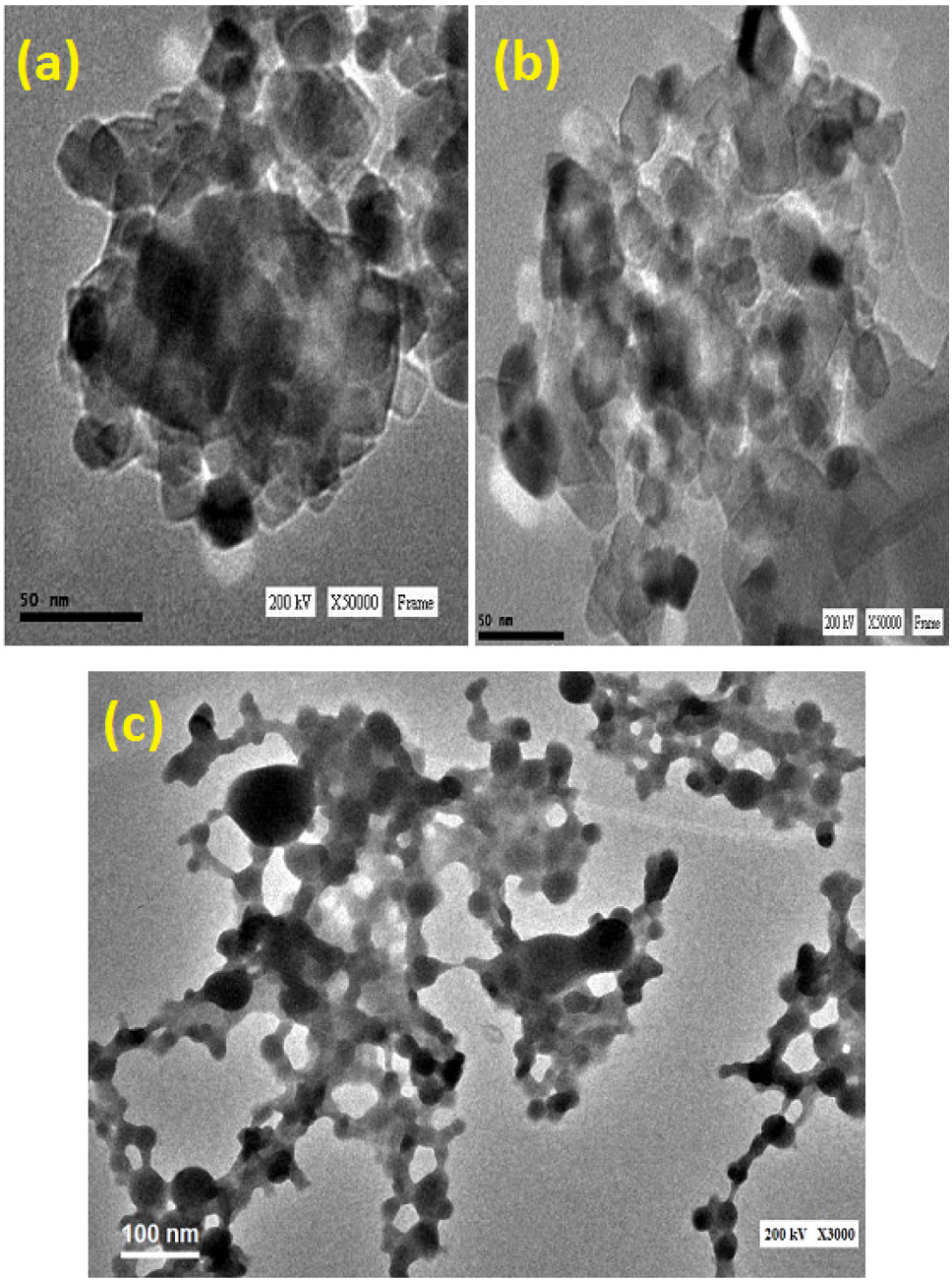

Fig. 2. (a,b) different TEM view of 1 wt.% PVA, (c) TEM after addition of P(AAc-*co*-AMPS) comonomer.

strongly ionizable $-SO_3$ groups (Souda and Sreejith, 2015; Ayman et al., 2010), so the AMPS (90 wt.%) was selected for adsorption in all experimental work.

3.4.2. *Effect of pH on adsorption of MB*

The adsorption of MB by both adsorbents were carried out in aqueous solution. The adsorption studies were carried out at pH 2–10 at room temperature. As shown in Fig. 6, even gel type's type possesses sensitivity towards the pH change. In the pH < 4, the removal of MB dye onto the gels is low, continuously increase with increasing pH values reached the maximum pH 6.0, and the positive charged of the MB dye in the solution has an affinity to functions with the net negative charges. When pH value has increased from 4 to 6 (above the pKa values of AAc = 4.2 and around 1.5 for AMPS) the ionic groups —OH, —COOH and $—SO_3H$ ionized to $—O^-$, —COO— and $—SO_3^-$ respectively, and this may be due to the formation of an ionic complex between MB dye molecules and the active sites in SIMT/CCPNT participate in chelation (Akl et al., 2016). Therefore, result the removal increase. The SIMT adsorbed less MB molecules due to low diffusion and lower surface area. At pH 6, the SIMT adsorbed 88.14 (mg/g) while 95.90 (mg/g) adsorbed by CCPNT nanogel type. At higher pH > 6, a screening agent of the counter ions, such as NH_4^+, Na^+, shielding the charges along the gel network type may clog up the active sites, thereby causing the decrease in dye removal (Ramazan and Ali, 2012).

3.4.3. *Adsorption kinetics*

Fig. 7 shows that the time required to achieve an equilibrium sorption of MB was 60 min for CCPNT while for SIMT at 100 min the equilibrium achieved. The internal pore diffusion and the overall available surface area of the CCPNT compared SIMT is the reason. The kinetics of adsorption consisted of two main portions: an initial

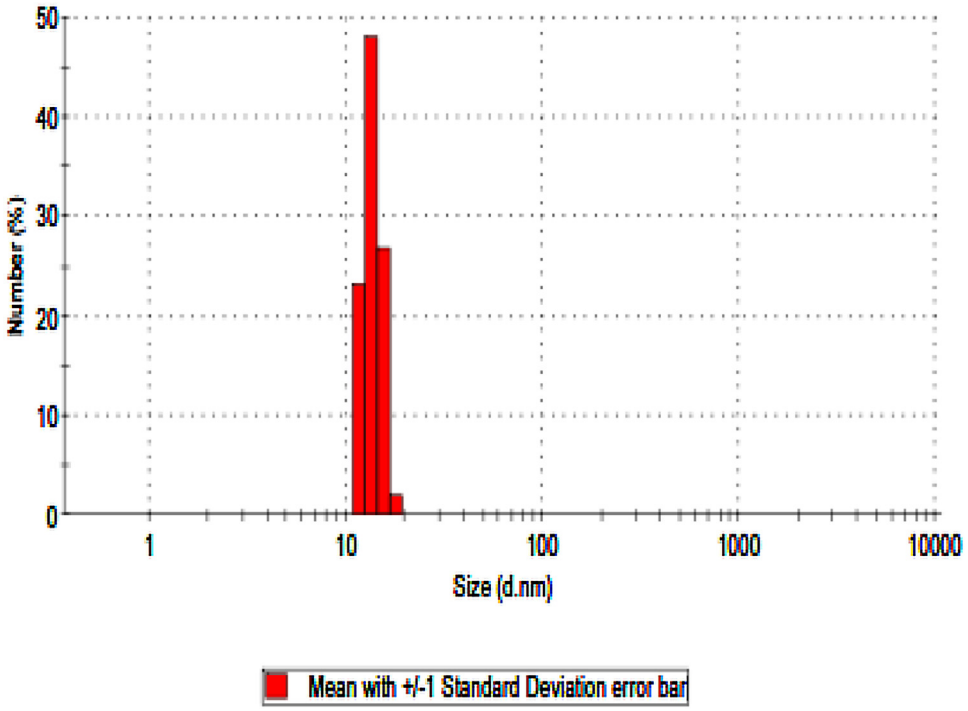

Fig. 3. Particle size distribution of CCPNT.

swift stage where adsorption was fast and contributed significantly to equilibrium uptake, and a slower second phase which assist to the total MB adsorption was relatively small i.e., intraparticle diffusion or chemical reaction would be the rate controlling step of sorption kinetics. The rapid uptake of MB may indicate that most of the active sites of the gels are exposed for interaction with the dye (Abdeen et al., 2015).

The kinetics of sorption can be followed using kinetic ensamples (pseudo-first, second-order kinetics and intraparticle diffusion) as expressed in the following equations:

$$\log(q_e - q_t) = \log q_e - \frac{k_1}{2.303} \quad (2)$$

$$\frac{t}{q_t} = \frac{1}{k_2 q_e^2} + \frac{t}{q_t} \quad (3)$$

$$q_t = k_p t^{0.5} + C \quad (4)$$

where the rate constants for pseudo-first is k_1 and that of second-order adsorption is k_2, the amount of MB adsorbed (mg/g) at equilibrium is q_e while the amount of MB adsorbed at time t is given as q_t, K_p (mmol. g^{-1} $h^{-0.5}$) is the intra-particle diffusion rate constant and C is a constant. For this model q_t versus $t^{0.5}$ may be linear if intra-particle diffusion is involved in the adsorption process (Sun and Yang, 2003). From equations given above the slope and intercept of the plot of t/qt with time t in Eq. (3) gives the values of the k_2 and the intercept is equivalent to the q_e. From Eq. (4), if pore diffusion is the rate limiting step, so a plot of q_t versus $t^{0.5}$ gives a straight line with a slope that equals k_p and the intercept value c exemplify the resistance to mass transfer inside the external liquid film. Fig. 8(a,b) illustrate the fitted results. The rate constants, amounts of adsorption equilibrium (q_e values) and correlation coefficients are computed in Table 2a. Apparently in Table 2a, the values of R^2 for both SIMT/CCPNT were found to be higher in the pseudo-second-order when it's being compared to the pseudo-first- order, else the q_e values obtained after computation through the pseudo-second-order equation indicate close agreement with those of the experimental q_e as shown in Table 2a, the pseudo-second-order indicates that the limiting step is chemical adsorption and the coefficient of correlation for the pseudo-second order almost equate to and this means the adsorbent have high adsorption capacity with short equilibrium time which shows a high degree of binding between the gel and the used dye.

Fig. 8(c) clarify that intraparticle diffusion plots are multi linear, the first portion is the transport of MB molecules from the depth solution to the adsorbent external surface by film diffusion. The second one is the diffusion of the MB molecules from the out surface into the pores of the adsorbent. The third portion is the meta stable equilibrium stage, where the MB molecules were covered the internal surface of the pores and the intra-particle diffusion springs to slowly due to the solute concentration in the solution getting lower (Sun and Yang, 2003). The separate intraparticle diffusion parameters are summarized in Table 2b. As seen from the data, the k_{p1} value is enhanced in the first stage, indicating improvement of the rate of adsorption by SIMT/CCPNT. Also, the $k_{p2,3}$ values of second and third linear portion are smaller than the first portion and this observation shows that the rate of dye adsorption at first section takes place faster. The high speed of adsorption at first part can be assigned to ease of availability of adsorption centers (Amr, 2012).

3.4.4. *Adsorption isotherm*

The effect of the MB concentration on the chelating ability of the prepared SIMT/CCPNT is an important parameter to define the efficiency of the gel types as a chelating material at low pollution levels. Fig. 9 shows a sharp increase in the adsorption capacity for CCPNT rather than SIMT, and then it tends to level off at higher concentrations (700 ppm). At initial step the adsorption capacity of nanogel increases nearly 3.8 folds as the solution concentration increases from 100 to 500 ppm. Whereas, less than 50% increment in the adsorption capacity as the feed solution concentration increased to 700 ppm. Such difference in the adsorption temper reveals the variety in the adsorption interactions that involves physical and chemical mechanisms (Gholam and Adeleh, 2013). The experimen-

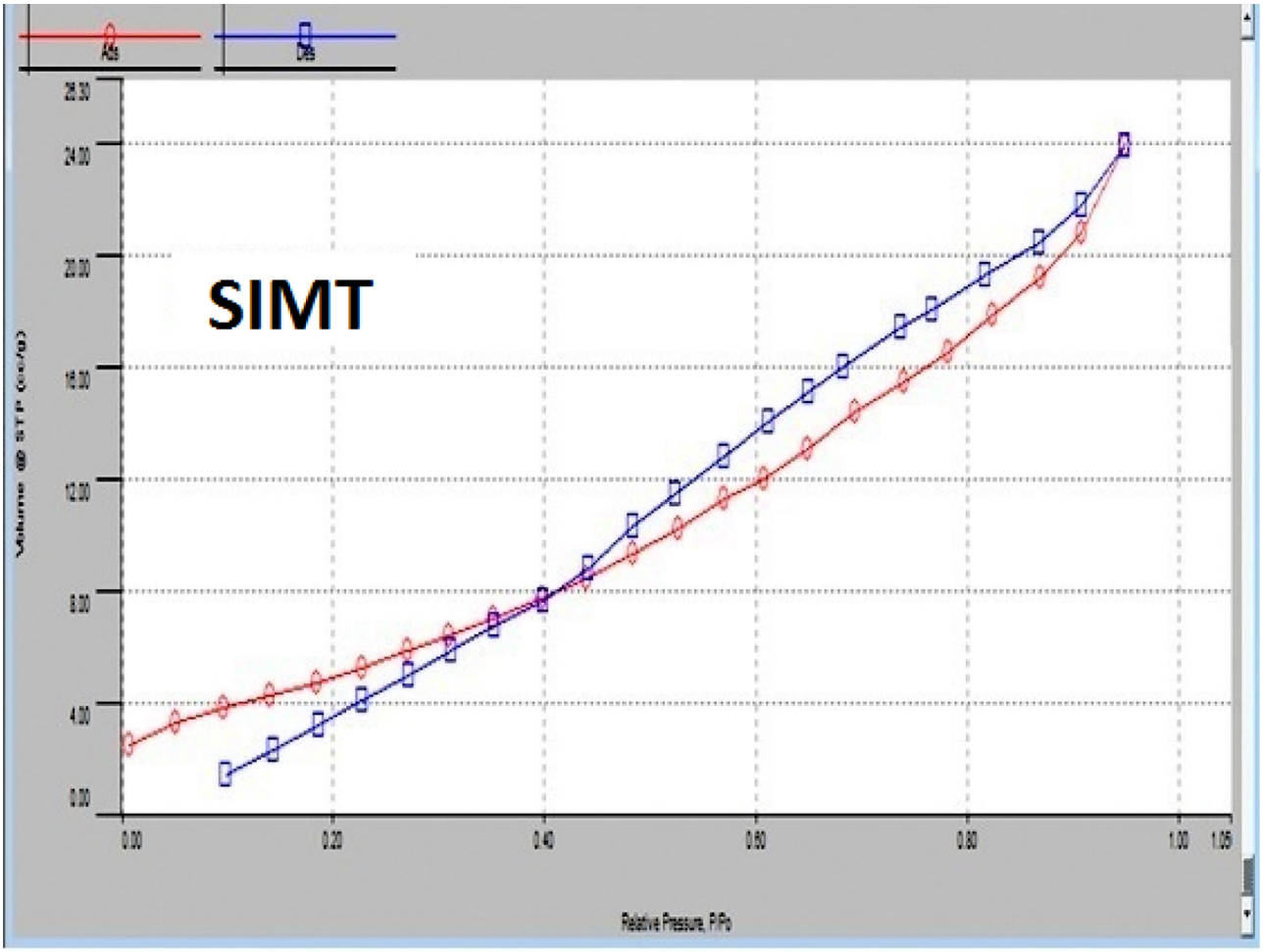

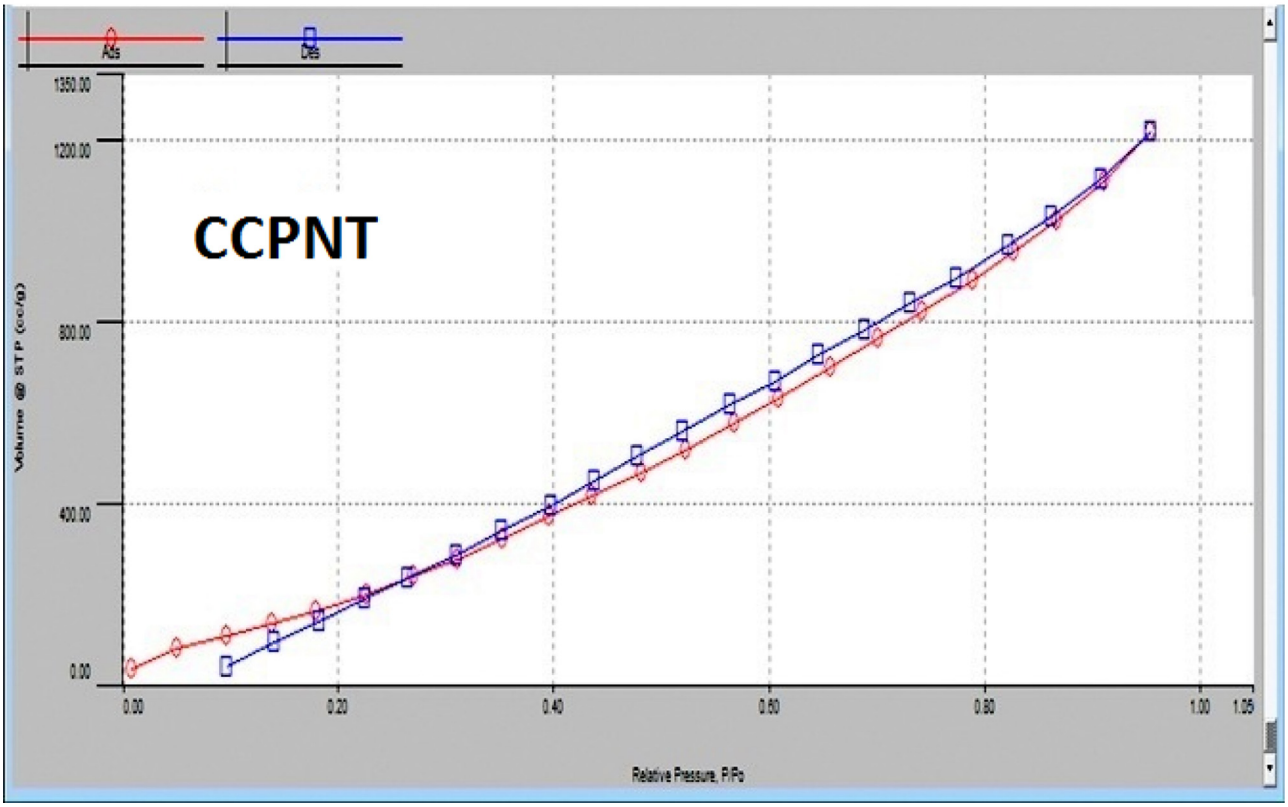

Fig. 4. Nitrogen sorption isotherms at 77 K for SIMT/CCPNT.

Table 2a
SIMT and CCPNT kinetic models parameter.

Gel Type	Pseudo-first-order			Pseudo-second-order			
	K_1 (min^{-1}) × 10^{-2}	R_1^2	q_{cal} (mg/g)	K (gmg^{-1} min^{-1}) × 10^{-3}	R_2^2	q_{cal}	q_{exp}
SIMT	3.5	0.9727	37.00	2.92	0.9991	90.09	19.8
CCPNT	7.5	0.8913	42.09	4.42	0.9998	98.03	18.8

Table 2b
Intra-particle diffusion adsorption constants for both SIMT/CCPNT.

Gel type	Intraparticle diffusion model					
	K_{p1}	R_1^2	K_{p2}	R_2^2	K_{p3}	R_3^2
SIMT	18.24	1	4.2	0.9477	1.8	0.9695
CCPNT	12.8	1	3.4	1	1.11	1

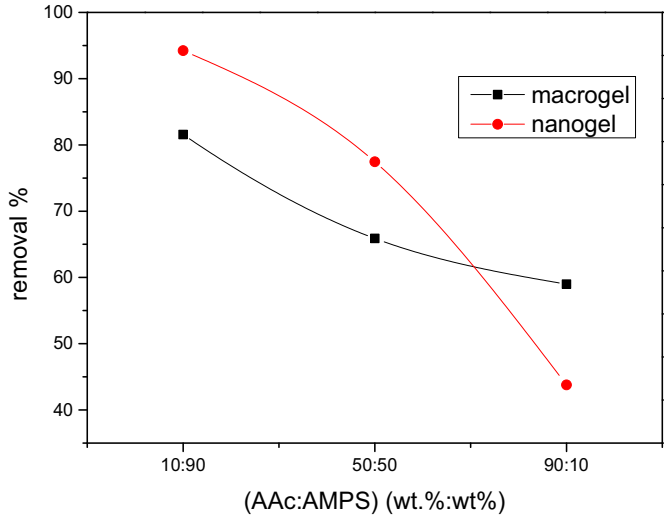

Fig. 5. Effect of monomer ratio on the adsorption amount of MB onto SIMT/CCPNT.

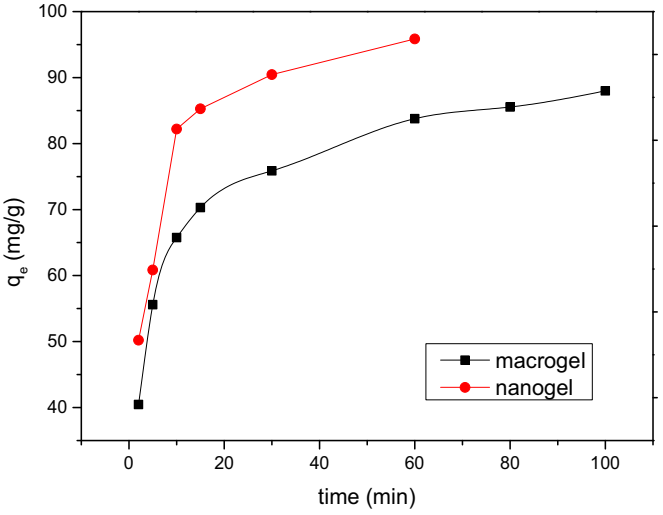

Fig. 7. Effect of contact time on adsorption.

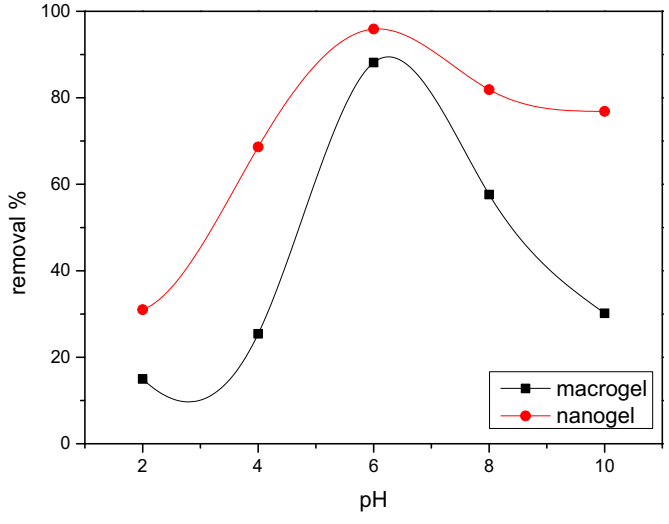

Fig. 6. Effect of pH on MB adsorption by SIMT and CCPNT.

tal data have been analyzed by the Langmuir model. The linear Langmuir equation is normally expressed as follows:

$$\frac{C_e}{q_e} = \frac{1}{k_l q_{max}} + \frac{C_e}{q_{max}} \quad (5)$$

where C_e (mg/l) and q_e (mg/g) are the equilibrium of MB dye concentrations in liquid and solid phase, respectively. q_{max} (mg/g) and k_L (mg/l) are Langmuir constants related to the monolayer adsorption capacity and adsorption binding energy, respectively, q_{max} and k_L can be calculated by plotting C_e versus C_e/q_e. A plot of C_e/q_e against C_e should give a straight line if the adsorption data conform to the Langmuir isotherm.

The second model applied in the analysis of data is the Freundlich model. The Freundlich model describes multilayer adsorption onto heterogeneous surfaces as contradictory with monolayer adsorption onto homogeneous surfaces according to the Langmuir model. The mathematical form of the Freundlich equation is given by

$$q = k_f C^n \quad (6)$$

q (mg/g) is the adsorbed amount; C (mg/l) the remaining solute concentration and K_f (L kg^{-1}) and n (dimensionless) are constants. The linearized form of the Freundlich equation is normally expressed as follows

$$ln q_e = \ln k_f + \frac{1}{n} \ln C_e \quad (7)$$

where q_e is the equilibrium adsorbed amount (mg/g); C_e is the saturated concentration of the adsorbate (mg/l); K_f and n are the Freundlich constants of the adsorption capacity and the rate of adsorption respectively. Fig. 10(a,b) represents the plot of the experimental data founded on Langmuir and Freundlich isotherms. Table 3, shows the calculated Langmuir and Freundlich model's parameters. The high values of correlation coefficients, R^2 (>0.999) for both SIMT/CCPNT, indicated that the equilibrium data were proposed better by Langmuir equation than by Freundlich equa-

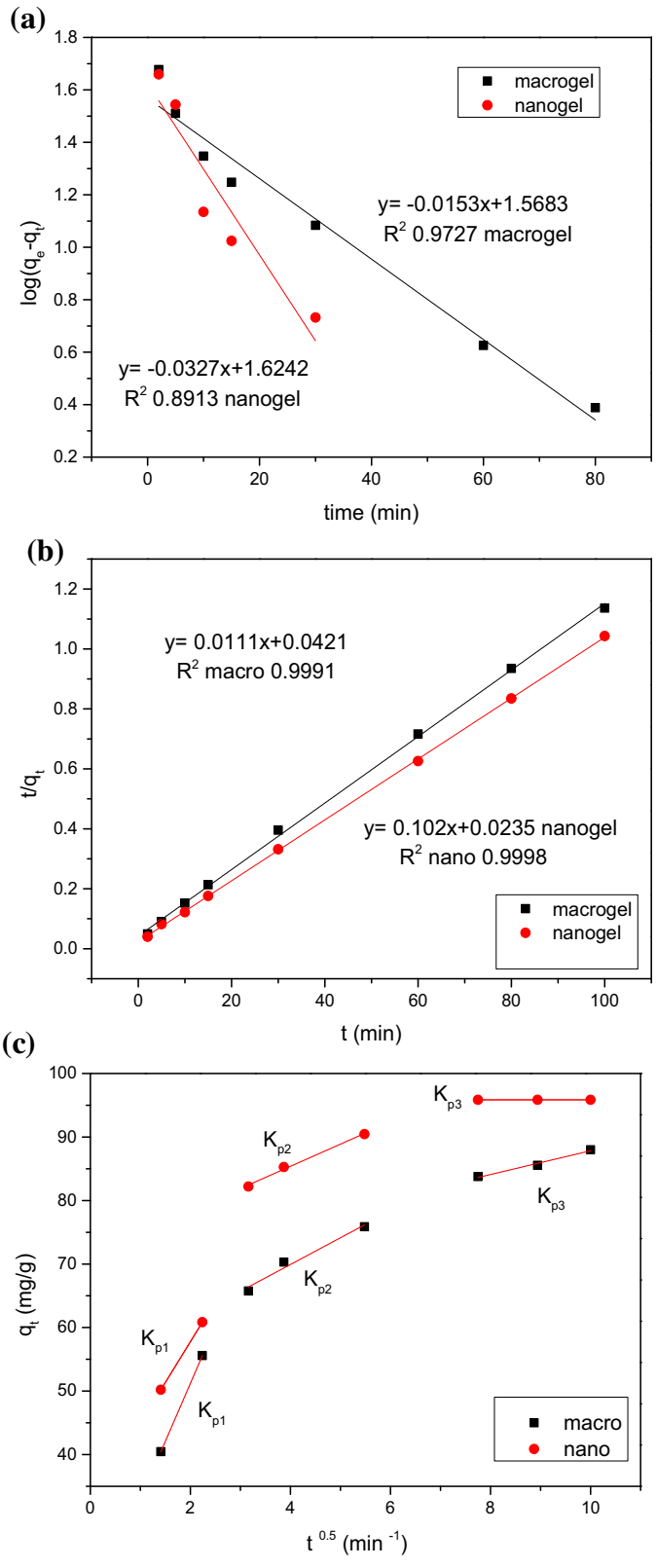

Fig. 8. (a) Adsorption kinetics of the MB onto the SIMT/CCPNT by the pseudo-first-order model, (b) kinetics of the MB by the pseudo-second-order model, (c) Intraparticle diffusion plots for the adsorption of MB onto SIMT/CCPNT.

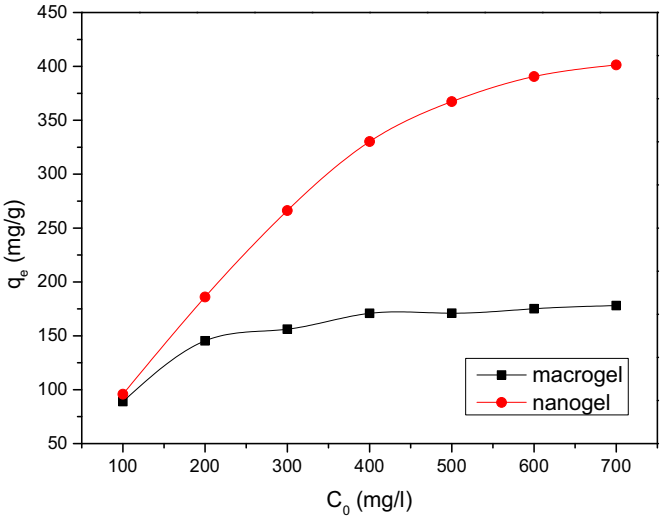

Fig. 9. Initial MB concentration effect on the adsorption uptake.

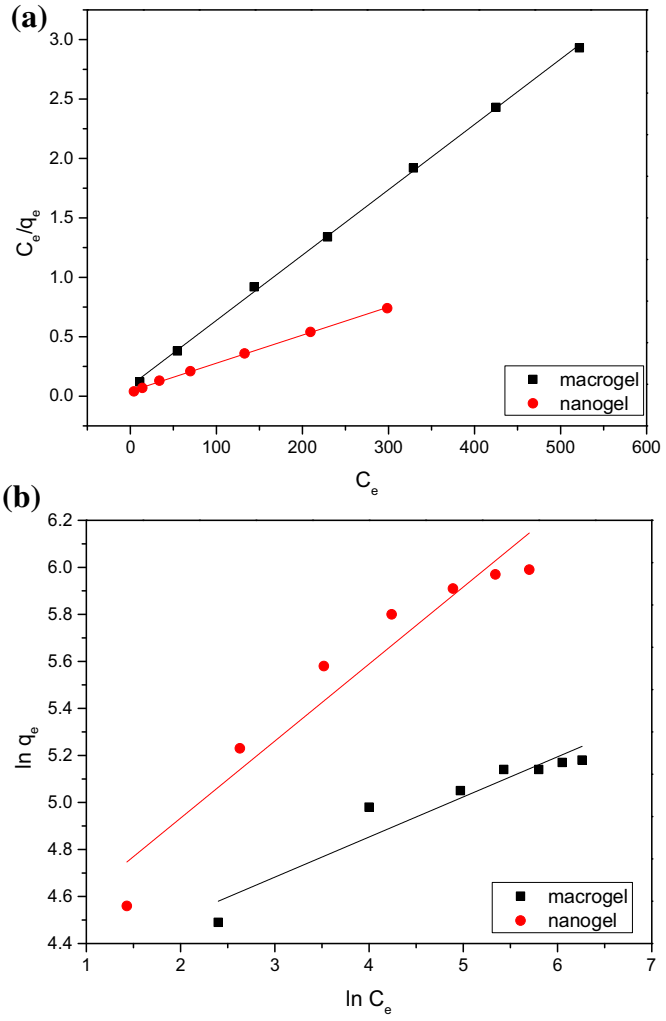

Fig. 10. (a) Langmuir adsorption isotherm on SIMT/CCPNT, (b) Freundlich isotherm of SIMT/CCPNT.

Table 3
Langmuir, Freundlich adsorption isotherm constant, correlation coefficient and q comparison.

gel code	Langmuir model			Freundlich model		
	K_L (min^{-1})	R_1^2	q_{cal} (mg/g)	q_{exp} K_f (mg/g)	R_2^2	1/n
SIMT	0.06	0.9994	178.07	181.8 1.42	0.9116	0.17
CCPNT	0.05	0.9997	401.3	416.6 1.45	0.9315	0.32

Table 4
Maximum adsorption capacities q_e (mg/g) for MB by some other adsorbents reported in literature.

Adsorbent	q_e (mg/g)	References
Fe_3O_4@APS@AA- *co*-CA MNPs	142.9	(Fei et al., 2012)
IPN (AAc-HEMA) Alginate-Na	172	(Mandal and Ray, 2013)
PAMPS/Chitosan hydrogel	74	(Akl et al., 2016)
Poly(NIPAAm/MA) hydrogel	322.6	(Betul et al., 2013)
Poly(acrylic acid) containing core–shell type resin	300	(Yavuz et al., 2011)
Chitosan hydrogel bead (CSB)	129.44	(Sudipta et al., 2011)
magnetite-loaded multi-walled carbon nanotubes (M-MWCNTs)	48.06	(Lunhong et al., 2011)
SIMT	181.8	This work
CCPNT	416.6	This work

Table 5
Thermodynamic factors for adsorption of MB by SIMT and CCPNT.

gel code	K_c				$-\Delta G^\circ$ (kJ/mol)				$-\Delta H^\circ$ (kJ/mol)	$-\Delta S^\circ$ (J/mol K)
	298 K	308 K	318 K	328 K	298 K	308 K	318 K	328 K		
SIMT	7.33	6.51	5.89	5.36	18.16	16.67	15.57	14.61	6.44	5.25
CCPNT	23.08	22.80	12.51	7.40	57.18	58.38	33.07	20.17	23.24	51.35

tion. Thus, the adsorption of MB on both SMT and CCPNT obeyed the Langmuir adsorption isotherm. From Table 3, the q_m values at optimum pH (~6) for SIMT/CCPNT were estimated to be 181.8 and 416.6 mg/g, respectively, The maximum amount of MB adsorbed by both network adsorbents is compared to other adsorbents published in literature shown in Table 4, The adsorption capacities of the synthesized gel types are comparatively higher than the other different polymer based adsorbents. Our results reveal the potential of these dynamics to be an effective Nano-adsorbent for removing basic dyes from aqua system.

3.5. Thermodynamic study

Thermodynamic parameters of the adsorption for the SIMT/CCPNT derived from 90 wt.% AMPS content in the both formulation were investigated. The Gibbs free energy can also be cleared using enthalpy and entropy at a constant temperature Eq. (9). The linear plot form Eq. (8) and (9) results in Eq. (10) which is the Van't Hoff equation (Mandal and Ray, 2013):

$$\Delta G^o = -RT\, lnk_c \tag{8}$$

$$\Delta G^o = \Delta H^o - T\Delta S^o \tag{9}$$

$$ln\, k_c = \frac{\Delta S}{R} - \frac{\Delta H}{RT} \tag{10}$$

where ΔG° (kJ mol^{-1}) is the change in Gibbs Free Energy, ΔH° (kJ mol^{-1}) is the enthalpy change of MB adsorption, ΔS° ($Jmol^{-1}$ K^{-1}) is the entropy change of MB molecule adsorption, (R) is the universal gas constant, while (T) is the absolute temperature (K) and K_c at three different temperatures i.e., 25, 35 and 50 °C were obtained from MB adsorption data at these different three temperatures for 100 mg/l feed concentration of MB. ΔH° and ΔS° were obtained from the slope and intercept of potting lnK_c with 1/T as in Fig. 11. Thermodynamic parameters of SIMT/CCPNT were calculated and are shown in Table 5. The results show that the adsorption of MB has a decreased randomness at the solid face/solution face, and is an exothermic and spontaneous nature because of the negative values of ΔS°, ΔH°, and ΔG°, respectively (Ngaha et al., 2011; Wu et al., 2014).

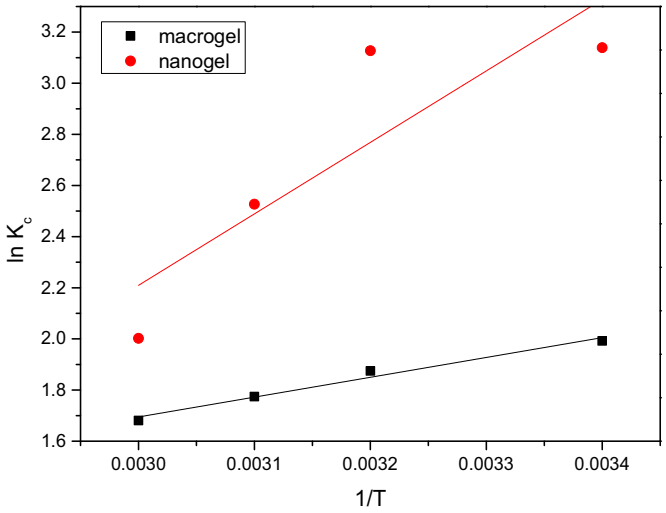

Fig. 11. Variation of ln K_c with temperature (1/T) for the adsorption of MB onto SIMT/CCPNT.

3.6. Regeneration and reuse of adsorbents

To detect the reusability of adsorbent, desorption experiment was conducted. The adsorbent was separated after adsorption study and dried well. The MB was desorbed for 3 h stirring in the presence of 0.1 M HCl and the adsorbents were dried at 40 °C. The recycled gels were used for next adsorption runs. The results of recycling experiment up to 6 cycles are shown in Fig. 12. One can see that the removal efficiency did not affect significantly even after six cycles of adsorption–desorption especially with nanogel and this may be due to the presence of hydrogel nanoparticles which facilitates separation and recycling of adsorbents.

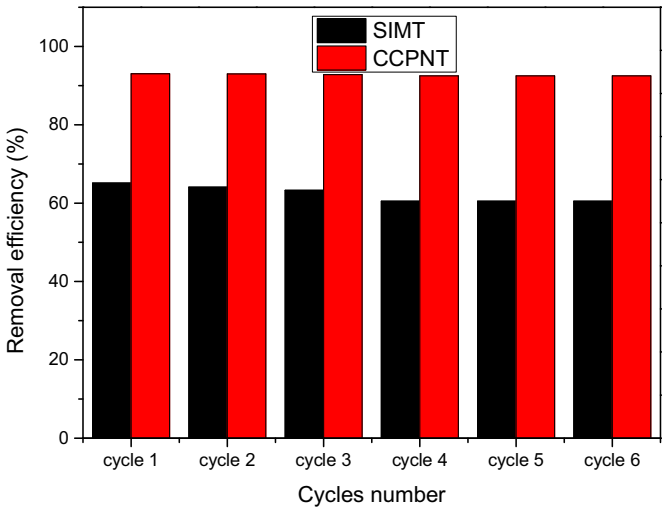

Fig. 12. Reusability of gel adsorbents.

4. Conclusion

In this work, PVA polymer matrix in two forms, SIMT/CCPNT based on comonomer (AAc-*co*-AMPS) were successfully synthesized. The gels surface was confirmed by SEM, TEM, DLS and BET analysis. The adsorption of MB on these adsorbents was found to be pH dependent. The kinetics of MB adsorption onto both networks followed the pseudo-second-order model. The adsorption of MB attained equilibrium within 60 min for nanogel and within 100 min for macrogel to reach 87–95% of MB being adsorbed. The equilibrium data were fitted well by the Langmuir isotherm model of adsorption. The maximum sorption capacities of MB for SIMT and CCPNT were 181.8 and 416.6 mg/g, respectively at pH 6 and 25 °C. The experimental results suggest that the SIMT/CCPNT could be employed as efficient and applicable adsorbents for the removal of MB cationic dye from wastewater.

Conflict of interest

The authors have declared no conflict of interest

References

Abdeen, Z., Mohammad, S.G., Mahmoud, M.S., 2015. Adsorption of Mn (II) ion on polyvinyl alcohol/chitosan dry blending from aqueous solution. Environ. Nanotech. Monit. Manag. 3, 1–9.

Akl, Z.F., El-Saeed, S.M., Atta, A.M., 2016. In-situ synthesis of magnetite acrylamide amino-amidoxime nanocomposite adsorbent for highly efficient sorption of U (VI) ions. J. Ind. Eng. Chem. 34, 105–116.

Allen, S.J., Koumanova, B., 2005. Decolourisation of water/wastewater using adsorption (review). J. Univ. Chem. Technol. Metal. 40, 175–192.

Amr, E.A., 2012. Removal of heavy metals from model wastewater by using carboxymehyl cellulose/2-acrylamido-2-methyl propane sulfonic acid hydrogels. J. Appl. Polym. Sci. 123, 763–769.

Auta, M., Hameed, B.H., 2012. Modified mesoporous clay adsorbent for adsorption isotherm and kinetics of methylene blue. Chem. Eng. J. 198, 219–227.

Ayman, M.A., Abd El Wahab, Z.H., El Shafey, Z.A., Zidan, W.I., Akl, Z.F., 2010. Characterization and evaluation of acrylic acid Co-2-acrylamido-2-methylpropane-sulfonic acid hydrogels for uranium recovery. J. Disper. Sci. Technol. 31, 1415–1422.

Betul, T., Erdal, O., Erol, K., 2013. Cationic dye adsorption by poly(*N*-isopropylacrylamide/maleic acid) copolymeric hydrogels prepared by gamma rays. J. Radioanal. Nucl. Chem. 298, 1469–1476.

Biffis, A., 2001. Functionalized microgels: novel stabilizers for catalytically active metal colloids. J. Mol. Catal A: Chem. 265, 303–307.

Chilkoti, A., Dreher, M.R., Meyer, D.E., Raucher, D., 2002. Targeted drug delivery by thermally responsive polymers. Adv. Drug Deliv. Rev. 54, 613–630.

Crini, G., 2006. Non-conventional low-cost adsorbents for dye removal: s review. Bioresour. Technol. 97, 1061–1085.

Dhara, D., Nisha, C.K., Chatterji, P.R., 1999. Superabsorbent hydrogels: interpenetrating networks of poly (acrylamide-*co*-acrylic acid) and poly (vinyl alcohol): Swelling behavior and structural parameters. J. Macromol. Sci. Part A: Pure Appl. Chem. 36, 197–210.

Dragan, E.S., Apopei, D.F., 2011. Synthesis and swelling behavior of pH-sensitive semi-interpenetrating polymer network composite hydrogels based on native and modified potatoes starch as potential sorbent for cationic dyes. Chem. Eng. J. 178, 252–263.

Fei, G., Hui, Y., Meng-Meng, L., Bao-Xiang, Z., 2012. Efficient removal of cationic dyes from aqueous solution by polymer-modified magnetic nanoparticles. Chem. Eng. J. 198, 11–17.

Gholam, R.M., Adeleh, A., 2013. Synthesis of kappa-carrageenan-*g*-poly(acrylamide)/sepiolite nanocomposite hydrogels and adsorption of cationic dye. Polym. Bull. 70, 2451–2470.

Gupta, V.K., Suhas, 2009. Application of low-cost adsorbents for dye removal: a review. J. Environ. Manage. 90, 2313–2342.

Hameed, B.H., Din, A.T.M., Ahmad, A.L., 2007. Adsorption of methylene blue onto bamboo-based activated carbon: kinetics and equilibrium studies. J. Hazard. Mater. 141, 819–825.

IUPAC Reporting Physisorption data, 1985. Pure Appl. Chem. 57, 603–613.

Jie, Y., Yuanpei, P., Quanfang, L., Wu, Y., Jinzhang, G., Yan, L., 2013. Synthesis and swelling behaviors of P(AMPS-*co*-AAc) superabsorbent hydrogel produced by glow-discharge electrolysis plasma. Plasma Chem. Plasma Process. 33, 219–235.

Jiuhui, Q., 2008. Research progress of novel adsorption processes in water purification: a review. J. Environ. Sci. 20, 1–13.

Kiser, P.F., Wilson, G., Needham, D., 2000. Lipid-coated microgels for the triggered release of doxorubicin. J. Control. Release 68, 9–22.

Lunhong, A., Chunying, Z., Fang, L., Yao, W., Ming, L., Lanying, M., Jing, J., 2011. Removal of methylene blue from aqueous solution with magnetite loaded multi-wall carbon nanotube: kinetic, isotherm and mechanism analysis. J. Hazard. Mater. 198, 282–290.

Magda, A.A., Ali, A.S., Kamel, R.S., Ayman, M.A., 2013. Application of crosslinked ionic poly(vinyl alcohol) nanogel as adsorbents for water treatment. J. Dispers. Sci. Technol. 34, 1399–1408.

Magdy, W.S., Riham, R.M., Eltaweel, S.H., Rania, S.S., 2012. Crosslinked poly(vinyl alcohol)/carboxymethyl chitosan hydrogels for removal of metal ions and dyestuff from aqueous solutions. J. Appl. Polym. Sci. 123, 3459–3469.

Mandal, B., Ray, S.K., 2013. Synthesis of interpenetrating network hydrogel from poly(acrylic acid-*co*-hydroxyethyl methacrylate) and sodium alginate: modeling and kinetics study for removal of synthetic dyes from water. Carbohydr. Polym. 98, 257–269.

Mandal, B., Ray, S.K., Bhattacharyya, R., 2012. Synthesis of full and semi interpenetrating hydrogel from polyvinyl alcohol and poly(acrylic acid-*co*-hydroxyethylmethacrylate) copolymer: study of swelling behavior, network parameters, and dye uptake properties. J. Appl. Polym. Sci. 124, 2250–2268.

Morris, G.E., Vincent, B., Snowden, M.J., 2016. The interaction of thermosensitive, anionic microgels with metal ion solution species. Prog. Colloid Polym. Sci. 105, 16–22.

Murray, M.J., Snowden, M.J., 1995. The preparation, characterization and applications of colloidal microgels. Adv. Colloid Interface Sci. 54, 73–91.

Ngaha, W.W.S., Teonga, L.C., Hanafiaha, M.A.K.M., 2011. Adsorption of dyes and heavy metal ions by chitosan composites: a review. Carbohydr. Polym. 83, 1446–1456.

Ömer, B.U., Semiha, K., Erdener, K., 2006. Polymeric absorbent for water sorption based on chemically crosslinked poly (acrylamide/2-acrylamido-2methyl-1-propanesulfonic acid sodium salt) hydrogels. Polym. Bull. 57, 703–712.

Pan, B.J., Pan, B.C., Zhang, W.M., 2009. Development of polymeric and polymer-based hybrid adsorbents for pollutants removal. Chem. Eng. J. 151, 19–29.

Peng, X.H., Wang, Y.J., Tang, X.L., Liu, W.S., 2011. Functionalized magnetic core-shell Fe_3O_4 @SiO_2 nanoparticles as selectivity-enhanced chemosensor for Hg(II). Dyes Pigments 91, 26–32.

Peppas, N.A., Bures, P., Leobandung, W., Ichikawa, H., 2000. Hydrogels in pharmaceutical formulations. Eur. J. Pharm. Biopharm. 50, 27–46.

Perez- Ameneiro, M., Bustos, G., Vecino, X., Barbosa- Pereira, L., Cruz, J.M., Moldes, A.B., 2015. Heterogenous lignocellulosic composites as bio-based adsorbents for wastewater dye removal: a kinetic comparison. Water Air Soil Pollut 226, 133–143.

Qu, J.H., 2008. Research progress of novel adsorption processes in water purification: a review. J. Environ. Sci. 20, 1–13.

Ramazan, C., Ali, D., 2012. Removal of methylene blue from aqueous solutions by poly(2-acrylamido-2-methylpropane sulfonic acid-*co*-itaconic acid) hydrogels. Polym. Bull. 68, 1889–1903.

Reese, C.E., Mikhonin, A.V., Kamenjicki, M., Tikhonov, A., Asher, S.A., 2004. Nanogel nanosecond photonic crystal optical switching. J. Am. Chem. Soc. 126, 1493–1496.

Risheng, Y., Jiajia, X., Xihua, L., Shengsong, D., 2011. Phase transition behavior of HPMC-AA and preparation of HPMC-PAA nanogels. J. Nanomater., 6, http://dx.doi.org/10.1155/2011/507542, Article ID: 507542.

Rivas, B.L., Quilodran, B., Quiroz, E., 2003. Removal properties of crosslinked poly(2-acrylamido glycolic acid) for trace heavy metal ions: effect of pH, temperature, contact time, and salinity on the adsorption behavior. J. Appl. Polym. Sci. 88, 2614–2621.

Shengfang, L., Xianli, L., Weidong, H., Wen, L., Xianyou, X., Shilin, Y., Jianying, Y., 2011. Magnetically assisted removal and separation of cationic dyes from

aqueous solution by magnetic nanocomposite hydrogels. Polym. Adv. Technol. 22, 2439–2447.
Souda, P., Sreejith, L., 2015. Magnetic hydrogel for better adsorption of heavy metals from aqueous solutions. J. Environ. Chem. Eng. 3, 1882–1891.
Sudipta, C., Tania, C., Seong-Rin, L., Seung, H.W., 2011. Adsorption of a cationic dye methylene blue, on to chitosan hydrogel beads generated by anionic surfactant gelation. Environ. Technol. 32, 1503–1514.
Sun, Q., Yang, L., 2003. The adsorption of basic dyes from aqueous solution on modified peat-resin particle. Water Res. 37, 1535–1544.
Vecino, X., Devesa-Rey, R., Villagrasa, S., Cruz, J.M., Moldes, A.B., 2015a. Kinetic and morphology study of alginate-vineyard pruning waste biocomposite vs non modified vineyard pruning waste for dye removal. J. Environ. Sci. 38, 158–167.
Vecino, X., Devesa-Rey, R., Cruz, J.M., Moldes, A.B., 2015b. Study of the physical properties of calcium alginate hydrogel beads containing vineyard pruning waste for dye removal. Carbohydr. Polym. 115, 129–138.
Wu, A.H., Jia, J., Luan, S.J., 2011. Amphiphilic PMMA/PEI core-shell nanoparticles as polymeric adsorbents to remove heavy metal pollutants. Colloids Surf. A: Phys. Eng. Asp. 384, 180–185.
Wu, R., Liu, J., Zhao, L., Zhang, X., Xie, J., Yu, B., Ma, X., Yang, S., Wang, H., Liu, Y., 2014. Hydrothermal preparation of magnetic Fe_3O_4@C nanoparticles for dye adsorption. J. Environ. Chem. Eng. 2, 907–913.
Yao, R.S., You, Q.D., Liu, P.J., Xu, Y.F., 2009. Synthesis and pH-induced phase transition behavior of PAA/PVA nanogels in aqueous media. J. Appl. Polym. Sci. 111, 358–362.
Yavuz, E., Bayramoğlu, G., Arica, M.Y., Senkal, B.F., 2011. Preparation of poly(acrylic acid) containing core–shell type resin for removal of basic dyes. J. Chem. Technol. Biotechnol. 86, 699–705.